

# Chapter 12

## Nanomaterials for Hydrogen Production Through Photocatalysis



Ahmed M. A. El Naggar, Mohamed S. A. Darwish  
and Asmaa S. Morshedy

**Abstract** In the last few decades, nanostructured materials have been of great interest worldwide due to their unique characteristics and their sub-driven reactivity. Furthermore, the unlimited applications of such materials in different fields and their associated success had added extra value for their importance. The combination between nanomaterials and photocatalytic processes has been recently given a great attention in different applications. It may enhance the viability of the nanotechnology principles. One of these applications is the usage of nanophotocatalytic materials in hydrogen production via water-splitting reaction. This chapter will cover the main concepts of photocatalysis and its associated terms. The main features of efficient photocatalysts and the ways of measuring such properties are illustrated in this chapter. Also, a brief presentation for the current methods that are utilized in the preparation of these catalysts is provided. An overview of the different types of semiconductors that are employed in the domain of photo-based hydrogen generation via splitting of water is introduced through this chapter too. A new approach in the water-splitting process by introducing noble metals attached magnetic nanoparticle (core/shell structure) as promising photomaterials is also described in this chapter. However, these materials are used in different fields such as bio-medical processes, water treatment, and energy storage. They are expected to be of high significance in field of catalysis, since they can be easily separated and recovered, due to their magnetic character, for reuse in further reactions. Implementation of a suitable magnetic force can enhance the hydrogen productivity during the water-splitting process. These materials are possessing magnetic properties which could reveal a new approach to their photocatalytic activity via quenching the radiation scattering.

**Keywords** Photocatalysis · Water-splitting processes hydrogen energy  
Magnetic materials · Semiconductors

---

A. M. A. El Naggar (✉) · M. S. A. Darwish · A. S. Morshedy  
Refining Department, Egyptian Petroleum Research Institute, Cairo, Egypt  
e-mail: [drmeto1979@yahoo.com](mailto:drmeto1979@yahoo.com)

© Springer Nature Singapore Pte Ltd. 2019  
S. Bhattacharya et al. (eds.), *Nano-Energetic Materials*, Energy, Environment  
and Sustainability, [https://doi.org/10.1007/978-981-13-3269-2\\_12](https://doi.org/10.1007/978-981-13-3269-2_12)

## Chapter Outline

This first part of this chapter illustrates the important definitions and terms of photocatalysis as well as the application of photo-based processes in various applications. The classifications and essential optical/ electronic characteristics of photocatalysts are reported in this part of the book. The relation between catalysts properties and proper irradiation sources is also discussed in details. An expanded overview of photocatalysis in water-splitting processes via two different routes is introduced in the second part of this chapter. The most common and efficient photocatalysts to generate hydrogen by splitting of water are also mentioned in this part.

## 12.1 Photocatalysis

Photocatalysis is a field of research that is developing fast with a great potentiality for use in various industrial applications, which include disinfection of air and water, mineralizing the organic contaminates, renewable fuels making, and organic creation. Photocatalysis is a word that was first known in Greece and consists of two pieces: photo (means: radiance) and the catalysis (partial break or decomposition). This term can be generally used to describe processes that are based on the light to activate a substance. The photocatalyst is a major item in such processes. It has been utilized to modify the rate of a chemical response without being involved in the chemical alteration. Therefore, conventional thermal catalyst is mainly different from a photocatalyst in the way of activation. Particularly, the first can be made under thermal effect, while second may be induced through light photons that have suitable power.

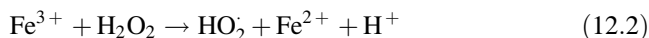
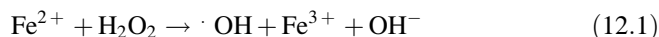
### 12.1.1 Types of Photocatalysis

Photocatalytic processes may occur in homogeneous or heterogeneous routes; however, heterogeneous photocatalysis has been rigorously investigated in past decades since it is highly likely to be used in versatile applications that are in relevance to environment, energy, and fabrication of organics.

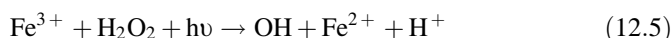
#### 12.1.1.1 Homogeneous Photocatalysis

In homogeneous photocatalysis, reacting species and catalysts are present in the same phase. Homogeneous photocatalysts that are of most common use includes photo-Fenton system ( $\text{Fe}^{2+}$  and  $\text{Fe}^{2+}/\text{H}_2\text{O}_2$ ). Reactive species in such media is  $\cdot\text{OH}$

radicals (Wu and Chang 2006) that are generated according to the subsequent mechanism (as shown in Eqs. (12.1)–(12.5)) (Ciesla et al. 2004).



In case of photo-Fenton course of action, extra supply of  $\cdot\text{OH}$  radicals should be taken into account. Specifically, hydroxyl radicals ( $\cdot\text{OH}$ ) are released through  $\text{H}_2\text{O}_2$ , photolysis, and consequent reduction of  $\text{Fe}^{+3}$  ions by the influence of UV irradiation; see Eqs. (12.4) and (12.5)



The effectiveness of Fenton-based processes may be affected by various operational factors such as hydrogen peroxide strength, pH, and radiation intensity (Wu and Chang 2006; Ciesla et al. 2004). The chief benefit of homogeneous photo-dependent methods is the possibility of using sunlight with radiation sensitivity around 450 nm; therefore, elevated expenditures of UV lamps and electricity can be avoided. These reactions could exhibit higher efficiency than diverse photocatalysis. On the other hand, a major drawback of this process is that it has to be carried out at low pH values. This obviously is due to the precipitation of Iron ions at increased pH values.

### 12.1.1.2 Heterogeneous Photocatalysis

In heterogeneous photocatalysis, the system entails the earlier configuration of a boundary between a solid photocatalyst and a fluid restrains reactants and outputs of the reaction. Interactions which involve lighted-up metal interfaces generally lie in the division of photochemistry.

So, concept of heterogeneous photocatalysis may basically be implemented in the processes that include a light-absorbing semiconductor in connection to liquid or gas phase. Although not all the heterogeneous photocatalysts are semiconductors, this type of solids is characterized of being most representative and broadly studied photoactive substances. So, it has been crucial to acquire some basic insights of physicochemical characteristics that belong to semiconductors and means of their interaction with radiation sources (Ciesla et al. 2004).

### 12.1.2 Electronic and Optical Properties of Heterogeneous Semiconductors

Semiconductors and insulators electronic individuality is of strong dependency to the band theory. Due to the huge number of atoms and their relevant electrons which act together in solid materials, equivalent levels of energy are spaced intimately forming bands. Each one of these energy band has its own level where the electrons occupy such bands from the level of minimum energy to the highest one. Latter statement is alike to the trend that electrons follow to engage orbitals of a certain atom (Moliton and Hiorns 2004).

The bands, of energy that are equivalent to engaged orbitals (HOMO) of the highest energy of definite molecule, are known as valance bands ( $V_B$ ). The following band that has higher energy capacity than  $V_B$  contains free orbital (LUMO) of this molecule. Therefore, this band is identified as conduction band ( $C_B$ ). Obviously, it can be said that  $V_B$  and  $C_B$  have been alienated via gap known as band gap ( $E_{bg}$ ). Hence, the classification of a solid material type as conductor, semiconductor, or insulator is related to its filled bands, size of its particles and band gap, as given in Fig. 12.1.

Generally, electrons can move within a solid species by applying an electric field if these species have a partially occupied or entirely empty band. On the other hand, electrical insulator has no possibility of electron flow as a result of the full occupation of  $V_B$  by electrons and the  $C_B$  is too far away in energy to be reached by its electrons. In conductors,  $V_B$  interferes with  $C_B$  (Park et al. 1995). Therefore, the electrons may transfer freely crossways all atoms of which the solid substance is made. In the case of semiconductor,  $E_{bg}$  is less than 4 eV. Thus, it can be bridged

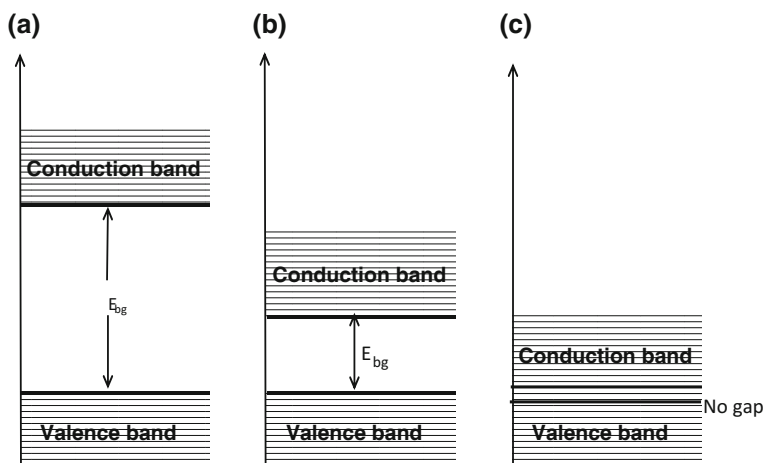


Fig. 12.1 Energy bands in solids: **a** insulator, **b** semiconductor and **c** conductor

either using thermal induction or light since these energy sources can encourage electrons movement from  $V_B$  to conduction band.

Semiconductors can be basically divided into two groups: intrinsic and extrinsic. The group of intrinsic semiconductors includes the undoped photoactive materials. Thus, the produced holes in  $V_B$  are formed under the effect of thermal excitation of electrons to subsequently reach to  $C_B$ . The behavior of such type of semiconductors is strongly dependent on surrounding temperature. For instance, no charge transfer for an intrinsic semiconductor can be attained at absolute zero ( $^{\circ}\text{K}$ ). Hence, semiconductors are changing to become as an insulator instead (Langot et al. 1996). At a finite temperature, electron ( $e^-$ ) of  $V_B$  may thermally depart to the  $C_B$ , creating behind vacant state in  $V_B$ , called a hole ( $h^+$ ). Electrons and holes are known as intrinsic charge carriers, and they usually move in opposite directions.

In intrinsic semiconductors, each electron in  $C_B$  has a parallel hole in  $V_B$ . Therefore, the number of electrons is always the same as that of holes. This number is symbolized as  $n_i$  and is called the intrinsic carrier concentration. An intrinsic semiconductor can be converted to extrinsic one through the insertion of impurity atoms into its crystal via an addition stage known as doping. Doping step makes a change in relative number of electrons and holes in the doped substance. This change has to be of strong dependency to type and inclusive number of doping atom (Perera et al. 1992). Chemical impurities that may involve their electrons to a conduction band are known as donors. Semiconductors that are doped by atoms of these donors can be assigned as n-type semiconductors. Electrons in n-type semiconductors (Shim and Guyot 2000) represent the majority of charge carriers where the number of electrons ( $n$ ) equals the number of involved atoms by donors. In contrary, holes are major charge carriers in p-type semiconductors (Chang and James 1989). The hole concentration ( $p$ ) in this type of semiconductors equals the concentration of acceptor atoms.

### 12.1.3 The Electronic Structure of Semiconductors

#### 12.1.3.1 The Fermi Energy Level

Fermi level,  $E_f$ , is of a vital consideration in the band theory. Electrons of solid materials are propagated in existing energy levels according to the statistics of Fermi–Dirac. These statistics describe potentiality of a given energy level ( $E$ ) to be filled with electron at a certain temperature. Fermi energy has been described as the needed energy to make the probability of occupying an energy level equals 0.5. However, the amount of this energy is strongly configured according to number of electrons in the system (Li et al. 2005). Exhibited Fermi level of intrinsic semiconductors (Fig. 12.2) can be seen as placed halfway between the  $C_B$  and  $V_B$  to show equal statistical potentiality to get a charge transporter through the two energy bands.

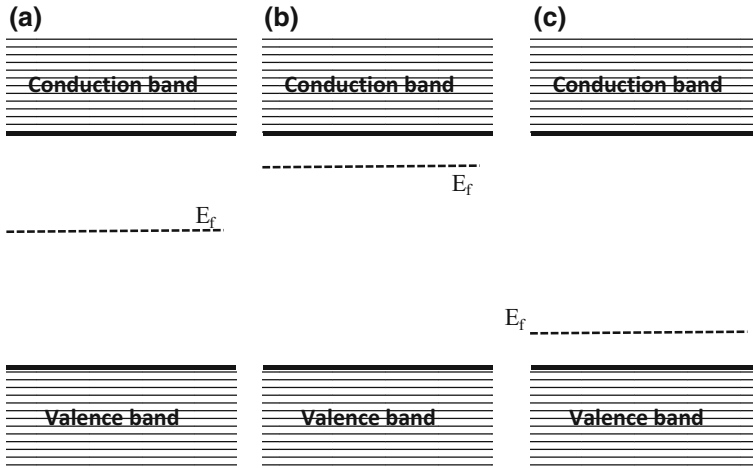


**Fig. 12.2** Location of Fermi level in relation to  $V_B$  and  $C_B$  for **a** intrinsic, **b** n-type, **c** p-type semiconductors

The insertion of donor impurities with the structure of an intrinsic semiconductor will consequently increase the chance of facing free electrons. Therefore, Fermi level makes a gradual move to be closer to  $C_B$  than the  $V_B$ . On the other hand, doping of an intrinsic semiconductor by acceptor impurities reduces the probability to come across free electrons. Nevertheless, potentiality to meet holes will be enhanced, and thus, the Fermi level reallocates to be nearer to the  $V_B$  than  $C_B$ .

### 12.1.3.2 Surface Versus Bulk Properties

Extinction of a semiconductor periodic structure at its free surface may get rid of its symmetry in a right-angle direction to the surface. This in turn may result in the creation of localized electronic state within the surface of semiconductor. This state may then affect the electronic features of surface which may by then play crucial effect through interaction between surface and adsorbed substances. Surface states can be presented as:

- (a) Existence of *dangling bonds*, i.e., superficial surface atoms that has no atoms above to bind with,
- (b) Surface reconstruction or relaxation, for example, variation of position and/or chemical bonding arrangement of surface atoms; hence, surface energy will be minimized,
- (c) Structural defects of the surface,
- (d) Adsorption of foreign atoms as impurity on surface,
- (e) Bonding involvement of the surface atoms and new phase atoms.

Energy levels that are positioned in the area of banned gap are of particular significance in terms of semiconductor optical properties. The manifestation of surface-localized states carries up movements of charge among core and surface of an atom in order to build up thermal balance between both of them. Thus, the density of charge delivery in environs of the surface moves away from its equilibrium value and makes the development of a non-neutral section in the bulk of semiconductor. This area is often identified as the surface space charge region (SCR). The features of bulk in pure semiconductors are improved at the rear of a few atomic layers in the core of their crystals. However, for doped semiconductors, the induction of surface states may lead to construction of a SCR that can go far (up to thousands angstroms) into the solid. Electrostatic potential, ( $V$ ), that might be obtained via the space charge region will subsequently make a development in the band configuration close to the surface, named as band bending. For n-type semiconductors, bands go up to the surface, while in p-type semiconductors, bands twist downward; these actions are due to the move of electrons from the surface region of donor to surface states in the first case, while in the second case, electrons transport from the surface states to acceptor. Work function (impact of surface electronic states and bending) of a doped semiconductor is non-relevant to the concentration of doping species. Particularly, doping of a semiconductor with donors inflates Fermi level; thus, work function of such semiconductor decreases. However, this effect can be stopped via elevating the energy spent by a skiving electron to pass over the SCR. This phenomenon in doped semiconductors has been called “pinning of Fermi level” (Walukiewicz 1988).

### 12.1.4 Ultraviolet and Visible Spectrometry

Absorption of an electromagnetic irradiation normally varies energy status of a molecule. These changes in state of energy include:

- Electronic state  $\Delta E_e = 150\text{--}600$  kJ/mol
- Vibrational state  $\Delta E_v = 2\text{--}60$  kJ/mol
- Rotational state  $\Delta E_r \approx 3$  kJ/mol.

The relation to the absorbed radiation wavelength is:

$$\Delta E = \Delta E_e + \Delta E_v + \Delta E_r = h\nu = h.c/\lambda$$

where (Planck’s constant)  $h = 6.626 \times 10^{-34}$  J s.

The energy gaps between molecular bonding, non-bonding, and anti-bonding orbitals lie in between 125 and 650 kJ per mole. This energy difference is due to the electromagnetic irradiation in both UV and visible regions of a spectrum (Perliski and Solomon 1993; Waymouth 1971; Sommerer 1996).

The UV–Visible spectrum can be split into three distinct regions:

1. Far UV (10–200 nm)
2. Near UV (200–380 nm)
3. Visible light (400–800 nm)

Dependent irradiation to each of the above-mentioned spectrum regions can just pass through certain types of glasswares. Table 12.1 summarizes values of potentially transmitting wavelength through some types of glass; hence, these types can be employed in photocatalytic reactions.

### 12.1.5 Radiation Sources

Good features of a spectrometric source can be represented through by a stable and high-intensity release. This in turn can provide such source with the capability to covers a broad range of wavelengths. Therefore, there is no specific single source that can be appropriate for all spectral zones. Irradiation sources can be categorized into thermal and electric discharge supply. Thermal radiations are generally resulting from elevating the operational temperature in a certain process. Hereafter, examples for some of the common irradiation sources are illustrated:

- *Deuterium discharge lamp*

This source uses an electrical discharge to dissociate deuterium molecules into atoms (Waymouth 1971). The process is accompanied by the emission of uninterrupted UV irradiation which lies nearly between 160 and 380 nm.

- *Tungsten filament lamp*

The most common source of visible radiation is the ordinary tungsten filament lamp. It is made from a thin spiral of tungsten string sealed inside an evacuated glass bulb. Electrical energy passing through the filament is converted to heat causing it to glow “white hot” (Waymouth 1971). *Mercury* is used under high pressure in Hg discharge tubes. Therefore, such source cannot be of proper use in spectral studies that are carried out with nonstop. This is obviously due to the sharp lines or bands that will be overlaid present on an unremitting background.

- *Xenon discharge lamp*

This lamp operates with a low-voltage DC source similar to that of the linear halogen lamp but at xenon pressures in the range of 10–30 atm. The intensity in the

**Table 12.1** Type of glass and their corresponding wavelength cut

| Type of glass | Wavelength cutoff (nm) |
|---------------|------------------------|
| Pyrex         | <275                   |
| Corex         | <260                   |
| Vycor         | <220                   |
| Quartz        | <170                   |



near UV is actually much greater than that of the LHL lamp, but even greater intensity in the visible region may pose potential stray radiation problems (Sommerer 1996).

- *Monochromators*

Monochromator is a source of radiation that can be utilized in order to disperse its chrome in reference to the desired wavelength. Prisms are broadly employed to attain such purpose. Glass, quartz, and fused silica are the most common materials to fabricate prisms are. Among those materials, glass could be counted as the highest of power resolving. This is because glass can firmly scatter light along the visible zone of a spectrum. Nevertheless, glass does not allow radiations that have wavelengths between 350 and 200 nm to transmit through. Thus, glass cannot be exploited at such range of wavelength. On the other hand, quartz usually permits wavelengths in the range of 200–700 nm to penetrate. Therefore, quartz is suitable for usage in UV region.

### ***12.1.6 Photocatalytic Metal Oxides***

In terms of molecular configuration, a metal oxide ( $\text{MO}_x$ ) consists of at least one metal atom combined with one or more oxygen atoms. Excluding a few of the lighter inert gases ([He], [Ne], [Ar], and [Kr]), virtually all other elements are capable of oxidation, especially metal elements. Metals tend to be highly conductive due to the presence of delocalized electrons within the material matrix. However, upon oxidation, metal atoms donate their electrons to oxygen species forming positive ions, thereby adopting an electropositive state. Metal oxides are generally classified as semiconductors because their conductivity is often dependent upon the level of external excitation (Wong and Fierro 2006; Cox 1996).

Typical applications of these metal oxide semiconductors (MOS) include transistors, resistors, light-emitting diodes, solar cells, gas sensors, and piezoelectric transducers. While predominantly found within the electrical and computer industry, MOS technology can also be found across several other industries including, chemical, mechanical, environmental, energy, and petroleum (Wong and Fierro 2006). An ideal photocatalyst for photocatalytic applications has to possess the following properties (Carp et al. 2004):

- (1) Stability of irradiation photons,
- (2) Inert toward chemical and biological substances,
- (3) Abundance and of low fabrication costs,
- (4) Ability to attract reacting species at appropriate photostimulation energy ( $h\nu \geq E_g$ ), where  $E_g$  represents energy band gap.

Several photocatalysts are lately modified for the utilization in multi-applications that can be induced by light irradiation. Photocatalysts/semiconductors that are of a

wide employment in different applications are generally oxide forms of transition metal. These metals oxides are commonly characterized by their unique features. Semiconductors always possess a void energy zone in which no levels of energy can be provided. Therefore, recombination between the generated electrons and holes via photoactivation in a semiconductor can be effectively prohibited (Ghosh and Rao 2004; Jing and Guo 2006; Selvam et al. 2011). Table 12.2 gives the band gaps values for some of the extensively utilized photocatalysts in various applications.

Cadmium oxide is considered one of astonishing compounds as a photocatalyst and some other application, for instance, its use as one of solar cells component (Salehi et al. 2014), phototransistors (Kondo et al. 1971), photodiodes (Benko and Koffyberg 1986), transparent electrodes (Chang et al. 2007), and gas sensors (Ghosh and Rao 2004). Another example for the cadmium compounds that are well known as efficient photocatalysts is cadmium sulfide. To best of knowledge, CdS has been counted as one of the most photoactive materials and is widely used in photocatalytic processes (El Naggar et al. 2013). On the other hand, although CdO may be taken into account as valuable photocatalyst, it has not been yet of extensive use. Cadmium oxide posses an exceptional feature based on owning a direct  $E_{bg}$  equal to 2.3 eV and indirect  $E_{bg}$  of 1.36 eV (Dou et al. 1998). CdO also holds a special catalytic aspect which makes it capable of photodecomposing various organic structures such as dyes and part of environmental contaminations (Nezamzadeh-Ejhih and Banan 2011; Karunakaran and Dhanalakshmi 2009; Karunakaran et al. 2010).

Another example of efficient photocatalytic oxides (that is of extensive use) is zinc oxide. Zn contains two electrons in its outer most valence shell. Due to its ability to form protective oxides, Zn is frequently utilized in rust preventive coatings. Zn is also commonly combined with other metals to form alloys such as brass when paired with copper (Taylor 1964; Bertini 2007).

ZnO is the most stable form; this inorganic compound can be found naturally in form of a yellowish mineral, known as zincite. It is considered a wide  $E_{bg}$  semiconductor at 3.37 eV and has a high excitation binding energy of 60 eV (Fan and Lu 2005; Ashfold et al. 2007; Kim et al. 2010). This semiconductor has been widely used for manufacturing white paints in pigment industry. ZnO can also

**Table 12.2** Example for excitation wavelengths of semiconductors and their matched energy of band gaps

| Examples for semiconductors | Band gap energy (eV) | Wavelength (nm) |
|-----------------------------|----------------------|-----------------|
| Titanium dioxide (rutile)   | 3                    | 413             |
| Titanium dioxide (anatase)  | 3.2                  | 388             |
| Zinc oxide                  | 3.2                  | 388             |
| Zinc sulfide                | 3.6                  | 335             |
| Cadmium sulfide             | 2.4                  | 516             |
| Cadmium oxide               | 2.1                  | 550             |

promote the catalytic fabrication of rubber stuff. With a moderately high refractive index ( $n = 2.0$ ), it is also added to polymers serving as a protectant from UV radiation (Zhang et al. 2004; Jacobson 2005; Hewitt and Jackson 2008).

Another example for one of the most common semiconductors is titanium oxide. Ti metal has been considered the ninth most plentiful constituent in earth crust at 6600 ppm by weight. Same as Zn, Ti forms a thin protective oxide layer when it is exposed to air in most environmental conditions (Taylor 1964; Bertini 2007). The most stable and most predominant form occurs as  $\text{TiO}_2$ , which is an inorganic chemical compound found naturally occurring as a white crystalline powder within magmatic rock and hydrothermal veins (Fu et al. 2009).

There are three main structural forms of  $\text{TiO}_2$ . Rutile and anatase have been the most widely spread phases having tetragonal crystal arrangements. Brookite, remaining less common, but still representative, exists in an orthorhombic crystal form. Ranging from 3.00 to 3.20 eV (depending on the wave factor),  $\text{TiO}_2$  is considered a moderately wide  $E_{\text{bg}}$  semiconductor with a reported binding energy between 45 and 55 eV (Hashimoto et al. 2005; Fujishima et al. 2008).

Due to its high refractive index ( $n = 2.7$ ),  $\text{TiO}_2$  is widely used as a whitening pigment and also provides the physical blocker in most sunscreens (Jacobson 2005).  $\text{TiO}_2$ , while highly effective at generating free radicals, is limited to activation energies of relatively high intensity (only found within the UV spectrum). Within the past few decades, significant progressions in metal oxide photocatalyst development have been made (Miyachi et al. 2002; Li et al. 2008; Brezesinski et al. 2010). However, titanium oxide maintains the vanguard of research interest as it continues to demonstrate the greatest photocatalytic promise. By hybridizing these two well-established metal oxides in the formation of heterogeneous nanostructures, it is anticipated that photocatalytic advancements can be realized (Moradi et al. 2015).

### ***12.1.7 Importance of Photocatalytic Efficiency of Metal Oxides by Nanostructure Growth Techniques***

The desire to fit more technology into smaller packages continues to push the scientific community to develop new and improved material designs. This trend is sustained through continued research in nanostructured materials. A material constrained to nanoscale dimensions offers unique properties that often behave starkly different from the same material in bulk form. As the feature's size shrinks, the effects of quantum mechanics begin to emerge. Vast increases in surface area show considerable potential for technological advancements, especially in energy applications. Understanding the behavior of metal oxide semiconductors at the atomic level continues to hold great interest within the research community. Several methodologies were improved through the past time to produce new as well as innovative MOS nanostructures including nanotubes, nanowires, nanorods,

nanoribbons, nanopropellers, and nanocoils (Fan and Lu 2005; Song et al. 2006; Tong et al. 2006). The most popular methods for producing these nanostructures include vapor–liquid–solid phase technique (VLS), pulsed laser deposition, hydrothermal growth (HG), and sputtering methods (Ashfold et al. 2007; Tak et al. 2009; Akhtar et al. 2010; Ottone et al. 2014; Smith et al. 2015). The precipitation synthesis can be considered one of the most potential techniques for creating uniform self-assembling growth patterns because it is inexpensive and effective. This method is promising for producing of a new photocatalytically predominant metal oxide nanostructure.

## 12.2 Hydrogen Production

Hydrogen as scalar quantity has been paid great attention lately. This attributed to its enormous content of energy as well as of being a clean source of energy generation. Several techniques have been currently utilized for hydrogen production such as pyrolysis and gasification of biomass wastes, catalytic decomposition of hydrocarbons, steam and dry reforming of ethanol and methane, respectively, and photocatalytic water splitting. However, taking into account the simplicity of production procedures and low energy consumption, the photocatalytic generation of hydrogen via cleavage of water molecules is favorable over the other methodologies. The hydrogen production by photocatalysis is often done through either the photocatalytic or photoelectrochemical crack of water.

### 12.2.1 Photocatalytic Water Splitting

Cleavage of water via photocatalytic route has been recently a perfect trend to obtain hydrogen especially through the utilization of two abundant renewable sources, specifically water and sunlight (Ni et al. 2007; Zheng et al. 2009). Usage of a proper photocatalyst in such process has to be an outstanding route due to the provided benefits which are as follows: Catalysts are introduced as solid phase, low costs of fabrication, no operational risks and against deactivation (Naik et al. 2011; Pradhan et al. 2011).

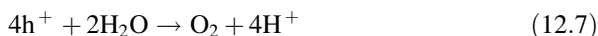
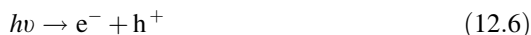
Improvement of a system for photo-induced breakup of water molecules that has the ability to use the zone of visible light in spectrum of sunlight can be carried out via various routes. One of these efficient routes has been dye sensitization. In this method, a dye sensitizer is inserted into a photocatalytic reactor. The sensitization is then excited due to the effect of visible irradiation. The molecules of dye sensitizer at excited state bring in electrons to the nearby  $C_B$  of a photocatalyst. These electrons transport afterward along the whole of photocatalyst crystalline structure.

These electrons will next reach to the catalyst surface and consequently attain the step of reducing water molecules to release hydrogen (Dhanalakshmi et al. 2001; Sreethawong and Yoshikawa 2012).

### 12.2.1.1 Semiconductors

Well-organized transfer of electrons in order to be received by molecules of a certain substrate is of a high relevance to the physicochemical features of semiconductors, such as specific surface area as well as crystalline and porous built-up. Generation of hydrogen via water cleavage through the usage of semiconductors has grabbed remarkable attention since the earlier work that had been done by Fujishima and Honda (1972). These scientists are the two who firstly explored that water molecule can be cracked down into hydrogen and oxygen via photoelectrochemical route. To achieve such process, a semiconductor electrode, namely  $\text{TiO}_2$ , had been utilized under the effect of UV rays. A great number of metals oxides and sulfides such as titanium dioxide (Karakitsou and Verykios 1995),  $\text{WO}_3$  (Abe et al. 2005), strontium titanate (Zou and Liu 2006), zinc oxide (Hoffman et al. 1992), cadmium and zinc sulfide (Maeda et al. 2005; Guan et al. 2004), niobates (Izumi et al. 1987), and tantalates (Furube et al. 2002) had been afterward presented as photocatalysts for obtaining hydrogen by splitting of water. In the last decade, scientists are paying attention to modify photocatalysts to enhance their capability toward the usage of irradiations that possess wavelengths ranged between 1400 and 700 nm. The modification stage includes doping of these catalysts by some of transition metal as platinum (Ikeda et al. 2006), chromium (Kim et al. 2005), and vanadium (Wang et al. 2006). The doping can also be carried out using non-metallic component, for example, nitrogen (Gu et al. 2007), sulfur (Yin et al. 2007; Murakami et al. 2007) as well as various carbon species (Yu et al. 2005; Liu et al. 2007). The modified photocatalysts could be by then efficient candidates for the generation of  $\text{H}_2$  via photocatalysis.

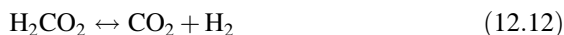
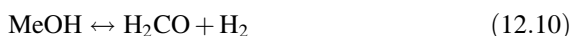
For an identical photoprocess to produce hydrogen, the potentiality of recombining the segregated charges during the photoreaction is of a strong dependence to the additives of water solution. Loading of metals onto the structure of semiconductor is another factor that can control the integration between separated charges. As soon as step of charge separation is completed, electrons in  $C_B$  can be confined via existing metals particles at the surface of semiconductors. Electron arrest at that stage is occurring as a result of the dissimilarity between Fermi energies and work function. In a process of hydrogen evolution from water, a solution contains both water and methanol is utilized. In such solution, the appearance of protons is taking place due to oxidation of either water or methanol via the radiation-produced holes. Protons are then obeying a reduction step, by electrons, at the metallic surface of catalyst in order to generate molecules of hydrogen. Equations (12.6)–(12.9) show the occurring interactions through the photocatalytic process of hydrogen formation (Choi and Kang 2007):



The overall reaction is



Methanol is added into the mixture to work as an oxidation mediator to prohibit the reveal of oxygen gas that may undertake due to adsorption of water molecules at the surface of photocatalyst. In other words, methanol has been employed to efficiently segregate the hole charges that are the reason behind the process of recombining hole–electron pair. Furthermore, methanol performs another role specifically as a hole scavenger. At this stage, methanol could take part in producing hydrogen, as presented in Eqs. (12.10)–(12.12). This subsequently develops the amount of total hydrogen gas productivity. In addition to the generated hydrogen, the occurring side reactions cause the production of carbon dioxide (Kawai and Sakata 1980; Chen et al. 1999).



### 12.2.1.2 Efficient Water-Splitter Catalysts

Cadmium sulfide is an n-type semiconductor that has an energy band gap of 2.4 eV. It is one of the photocatalysts that exhibited a reasonable photocatalytic action toward  $H_2$  generation in the presence of visible light irradiation. However, the use of  $C_2H_5OH$ ,  $HS$ , or  $SO_3$  (Sathish et al. 2006), as sacrificial electron donors, is highly advised to acquire significant amounts of  $H_2$ . It is also favorable to overcome the photo-induced corrosion of cadmium sulfide in attendance of  $O_2$ . From another perspective, electronic states as well as photoactivity of a semiconductor generally and cadmium sulfide in particular can be adjusted through varying or managing its crystals size with no influence on chemical structure. Hoffman and co-authors had stated an increment, by tenfolds, in efficiency of ZnO nanoparticles toward photocatalytic making of  $H_2O_2$  by decreasing the crystal size of semiconductor from 40 to 23 nm. Another study by Hoffman et al. (1994) had reported the increase in quantum competence in photopolymerization of methyl methacrylate with a parallel decline of crystal size via utilization of size-quantized particles of cadmium sulfide.

Combining two or more semiconductors that have various energy levels can be advantageous to attain successful charge disconnection.

Designation of nanocomposite structures had been of much interest owing to their enhanced response in both UV and visible light zones versus photo-based processes (Morales-Torres et al. 2012, 2013).  $\text{TiO}_2$  is well thought-out as the photocatalyst of highest activity. Nevertheless, the usage of  $\text{TiO}_2$  in photocatalytic cracking of water is dependent on its redox potential with consideration for the normal hydrogen electrode (NHE) (Pérez-Larios and Gómez 2013). Several investigations were previously carried out in order to elevate the photocatalytic performance of  $\text{TiO}_2$  toward the reaction of splitting water molecules. An improved structure of  $\text{TiO}_2$  had been obtained through doping with iron, zinc, copper, vanadium, magnesium, and nickel (Tseng and Jeffrey 2004). Another way of modifying titanium dioxide was done by impregnating its particles with precious metals such as platinum, palladium, and gold, as reported in Sreethawong et al. (2005).

The presentation of mixed oxide-based photocatalysts has also grabbed the attention of many scientists. These mixed structures may simultaneously contain two or more metals oxides, for example, the combination between at least two of the following oxides: copper oxide, zinc oxide, nickel oxide, and cerium oxide (Erdőlyi et al. 2006; Yoong et al. 2009; César et al. 2008; Banerjee 2011; Galindo-Hernández and Gómez 2011). Mixed oxide-based photocatalysts had displayed outstanding photocatalytic efficiency and are counted as materials of low fabrication expenses. The influence of combining two oxides or more has been of strong relevance to existing oxygen vacancies in their crystal structure (Nakamura et al. 2000; Ihara et al. 2003). El Nagggar and co-authors had demonstrated in a prior study (El Nagggar et al. 2013) the photocatalytic cleavage of water to evolve hydrogen from water–methanol mixture in the presence of zinc oxide ( $E_{\text{bg}}$  of 3.37 eV) and cadmium sulfide ( $E_{\text{bg}}$  of 2.42 eV) either separately or combined together. It had been explicitly mentioned that CdS and ZnO have distinctive performance toward photocatalytic conversion of water into hydrogen, in the occurrence of either UV or visible spectrums.

### ***12.2.2 Photoelectrochemical Hydrogen Production***

In photoelectrochemical process, hydrogen is produced using sunlight through water splitting at a semiconducting material by direct conversion of solar to chemical energy, particularly the hydrogen gas.

The most challenging task in generating hydrogen via photocatalytic cleavage of water molecules is to maximize amount of produced  $\text{H}_2$  via a cost-effective process. Improvements are required in cost, efficiency, and immovability for market viability as:

- Efficiency is being improved through better surface catalysis to enhance sunlight absorption.
- Immovability is being amended with rugged and protective surface coatings.
- Cost-effective is being lowered through reduced materials and processing costs.

The arrangement of a semiconductor electrode may have a considerable impact on the performance of photoelectrochemical cracking of water. Different semiconductor compositions, for instance,  $\text{TiO}_2$ ,  $\alpha\text{-Fe}_2\text{O}_3$ , and  $\text{WO}_3$  were investigated in hydrogen evolution by photoelectrochemical process (Cha et al. 2011; Kim et al. 2012). Heterojunction electrodes (has at least two or various photocatalysts) suggest better benefits when compared with single semiconductor electrode (Hoshino et al. 2006). CdS/ZnSe nanocore/shell photoelectrodes were prepared recently by Hyun et al. CdS/ZnSe exhibited increased photocatalytic features in comparison to thin film of CdS photoelectrodes. The band structure had stimulated the charge separation of carriers in the semiconductor electrodes and in turn could speed up the water-splitting process at lower and at higher bias voltages compared to CdS thin-film electrodes (Ki and Yun 2017). The photocatalytic hydrogen ( $\text{H}_2$ ) production activities of various CdSe semiconductor nanoparticles were investigated and compared including CdSe and CdSe/CdS quantum dots (QDs), CdSe quantum rods (QRs), and CdSe/CdS dot-in-rods (DIRs). The rate of  $\text{H}_2$  production orders as CdSe QDs  $\gg$  CdSe QRs > CdSe/CdS QDs > CdSe/CdS DIRs. Calculations of photoexcited surface charge densities are positively correlated with the  $\text{H}_2$  production rate and found that the efficiency of  $\text{H}_2$  production effected mainly by the size and morphology of the nanoparticle (Fen et al. 2016). In another report, the hydrogen production rate increased more than 4 times after the deposition of Ru on the surface of ZnS-CdS. In addition, the as-prepared ZnS-CdS nanocomposite demonstrated an excellent stability over 50 h (Jingyi 2017).

The use of an embedded structure, where one ingredient is surrounded by another, creates a larger contact area for electrons to be transferred more freely, thereby better realizing a synergistic effect in the heterojunction system. The Si-doped and Ti-doped  $\alpha\text{-Fe}_2\text{O}_3$  exhibited much higher photoelectrochemical activity than the undoped material. The proposed mechanism for the enhanced photocurrent is reduction of recombination due to an improvement of the charge-transfer rate coefficient at the surface and also possibly passivation of the grain boundaries by the dopants (Glasscock et al. 2007). Carbon-doped  $\text{In}_2\text{CO}_3$  films were fabricated with spray pyrolysis and estimated for photoelectrocatalysis. Photocurrent densities go up to  $1 \text{ mA/cm}^2$  for the C-doped films, with a high contribution from visible light irradiation. An enhanced photocurrent density has been observed for C-doped  $\text{In}_2\text{O}_3$  than the undoped films, with the same irradiation conditions (Yanping et al. 2008). Recently, Cu-doped ZnS/zeolite composites have been synthesized and subsequently evaluated for their photocatalytic activities based on hydrogen production from an aqueous  $\text{S}^{2-}/\text{SO}_3^{2-}$  solution under UV-visible light irradiation. It was found that the hydrogen production rate over CuZnS/zeolite composites was significantly higher than over the bulk ZnS (Toru and Morio 2017). To date, a variety of nanostructures with large structural voids and surface



areas have been fabricated, including nanoparticles, nanorods, nanotubes, and nanowires. The efficiency of silicon for hydrogen production can be improved by developing the antireflective property of nanosilicon substrate. Silicon nanowires coated with an iron sulfur carbonyl catalyst produced much greater photocurrent densities ( $-17 \text{ mA/cm}^2$ ) when compared to bare silicon nanowires ( $-5 \text{ mA/cm}^2$ ). In addition, the amount of hydrogen gas was produced ( $315 \text{ }\mu\text{mol/h}$ ) at low bias potentials for the silicon nanowires coated with an iron sulfur carbonyl catalyst (Soundarrajan et al. 2016). The SiC-TiO<sub>2</sub>-Sm<sub>2</sub>O<sub>3</sub> was fabricated by solgel process and thermal process at  $600 \text{ }^\circ\text{C}$  with different contents of samarium. It was reported that hydrogen was produced on SiC-TiO<sub>2</sub>-Sm<sub>2</sub>O<sub>3</sub> from a sulfuric acid solution by applying a bias potential with UV light. The results showed a maximum value of percentage of incident photon conversion efficiency (% IPCE = 4.7) for the sample with 2.0 wt% of Sm<sup>3+</sup> ions (Isaías et al. 2015). WO<sub>3</sub>/BiVO<sub>4</sub> heterojunction is considered one of the best pairs for hydrogen production, but its photocurrent density is scanty. The advantage of using helical nanostructures in photoelectrochemical solar water splitting was investigated. Bismuth vanadate-decorated tungsten trioxide helical nanostructures lead to the highest photocurrent density at 1.23 V versus the reversible hydrogen electrode as a result of the combination of effective light scattering, charge separation and transportation, and an enlarged contact surface area with electrolytes (Xinjian et al. 2014). The fabrication of CdSe quantum dot-sensitized photocathodes on NiO-coated indium tin oxide (ITO) electrodes for hydrogen production upon light irradiation was reported. The rainbow photocathodes with forward energetic gradient for charge separation and subsequent electron transfer to a solution-based hydrogen-evolving catalyst show good light harvesting ability and improved photoresponses than the reverse rainbow photocathodes under white LED light illumination. Under minimally optimized conditions, a photocurrent density of as high as  $115 \text{ }\mu\text{A cm}^{-2}$  and a Faradaic efficiency of 99.5% are achieved; this is among the most effective QD-based photocathode water-splitting systems (Hongjin et al. 2017). A novel configuration of the photoelectrochemical hydrogen production device is based on TiO<sub>2</sub> beads as the primary photoanode material with the addition of a heterostructure of silver nanoparticles/grapheme. The heterostructure not only caters to a great improvement in light harvesting efficiency (LHE) but also enhances the charge collection efficiency. The PCE of the TiO<sub>2</sub> beads/Ag/grapheme cell is improved 2.5 times than for pure P<sub>25</sub> cell (Chun-Ren et al. 2016). Pt and grapheme (GN) were used to modify TiO<sub>2</sub> nanoparticles. GN/TiO<sub>2</sub> (TG), Pt-TiO<sub>2</sub> (PT), Pt-GN/TiO<sub>2</sub> (PTG) and have been investigated in hydrogen production. The maximum hydrogen production rate was approximately  $4.71 \text{ mmol h}^{-1} \text{ g}^{-1}$  when the Pt content was 1.0 wt%. The situation of grapheme is similar to Pt. The highest hydrogen production rate is  $6.58 \text{ mmol h}^{-1} \text{ g}^{-1}$  by 1.5 wt% Pt-5 wt% GN/TiO<sub>2</sub> (1.5PTG5), which is about 1.4 and 2.2 times higher than that of Pt-TiO<sub>2</sub> and GN/TiO<sub>2</sub> binary composites, respectively (Nguyen et al. 2018).

Using of noble metals/magnetic nanoparticle (core/shell structure) as photomaterials is promising in water-splitting process. The rate of hydrogen production can be enhanced with magnetic heating of noble-metal-free catalysts. Using nickel/iron

carbide core–shell, which are exposed to magnetic heating with high-frequency magnetic field, an over potential (at  $20 \text{ mA cm}^{-2}$ ) declined by 200 mV is needed for oxygen generation in an alkaline water-electrolysis flow-cell, while for hydrogen production it had been decreased by 100 mV. Enhancement of oxygen-release kinetics has corresponded to an increase of cell temperature to  $\sim 200 \text{ }^\circ\text{C}$ ; however practically, it had elevated by  $5 \text{ }^\circ\text{C}$  only (Christiane et al. 2018).

## 12.3 Conclusion

The presented chapter reported at the beginning the definition, importance, and the types of photocatalysis. The electronic and optical characteristics of photocatalytic semiconductors had been then overviewed in details. Energy band gaps of the different semiconductors and their relevant type of irradiation spectrums had been widely discussed. The suitability of the various glass types and their matching to the radiation sources has been also presented through this chapter. The various metals oxide-based semiconductors had been reported as the most efficient and utilized photocatalysts in the versatile applications. Among these metals oxides, the titanium, zinc, and cadmium oxides have been listed as the photocatalysts of the highest activity in general and energy production in particular. One of the distinctive usages for the photocatalysis especially for the subject of energy generation, namely photocatalytic water conversion into hydrogen, was described in this chapter. Importance of water-splitting process in order to generate hydrogen is also illustrated taking into account that hydrogen has been counted as one of remarkable new energy vectors. Two routes of water splitting, photocatalytic and photoelectrochemical, and their dependent photocatalysts are also presented. The efficiency of various semiconductors through the two routes of splitting process is displayed through this chapter.

## References

- Abe R, Takata T, Sugihara H, Domen K (2005) Photocatalytic overall water splitting under visible light by TaON and  $\text{WO}_3$  with an  $\text{IO}_3^-/\text{I}^-$  shuttle redox mediator. *Chem Commun* 30: 3829–3831
- Akhtar MS, Hyung JH, Kim DJ, Kim TH, Lee SK, Yang O (2010) A comparative photovoltaic study of perforated ZnO nanotube/ $\text{TiO}_2$  thin film and ZnO nanowire/ $\text{TiO}_2$  thin film electrode-based dye-sensitized solar cells. *J Korean Phys Soc* 56(3):813–817
- Ashfold MNR, Doherty RP, Ndifor-Angwafor NG, Riley DJ, Sun Y (2007) The kinetics of the hydrothermal growth of ZnO nanostructures. *Thin Solid Films* 515:8679–8683
- Banerjee AN (2011) The design, fabrication, and photocatalytic utility of nanostructured semiconductors: focus on  $\text{TiO}_2$ -based nanostructures. *Nanotechnol Sci Appl* 4:36–65
- Benko FA, Koffyberg FP (1986) Quantum efficiency and optical transitions of CdO photoanodes. *Solid State Commun* 57:901–903
- Bertini I (2007) *Biological inorganic chemistry: structure and reactivity*, chap. 2. University Science Books, pp 7–30

- Brezesinski K, Ostermann R, Hartmann P, Perlich J, Brezesinski T (2010) Exceptional photocatalytic activity of ordered mesoporous  $\text{TiO}_2\text{-Bi}_2\text{O}_3$  thin films and electrospun nanofiber mats. *Chem Mater* 22:3079–3085
- Carp O, Huisman CL, Reller A (2004) Photoinduced reactivity of titanium dioxide. *Prog Solid State Chem* 32:33–177
- César DV, Robertson RF, Resende NS (2008) Characterization of ZnO and  $\text{TiO}_2$  catalysts to hydrogen production using thermoprogrammed desorption of methanol. *Catal Today* 133: 136–141
- Cha HG et al (2011) Facile preparation of  $\text{Fe}_2\text{O}_3$  thin film with photoelectrochemical properties. *Chem Commun* 47:2441–2443
- Chang YC, James RB (1989) Saturation of intersubband transitions in p-type semiconductor quantum wells. *Phys Rev B* 39:12672
- Chang J, Mane RS, Ham D, Lee W, Cho BW, Lee JK, Han S-H (2007) Electrochemical capacitive properties of cadmium oxide films. *Electrochim Acta* 53:695–699
- Chen J, Ollis DF, Rulken WH, Bruning H (1999) Photocatalyzed oxidation of alcohols and organochlorides in the presence of native  $\text{TiO}_2$  and metallized  $\text{TiO}_2$  suspensions. Part (II): photocatalytic mechanisms. *Water Res* 33:669–676
- Choi H-J, Kang M (2007) Hydrogen production from methanol–water decomposition in a liquid photosystem using the anatase structure of Cu loaded  $\text{TiO}_2$ . *Int J Hydrogen Energy* 32: 3841–3848
- Christiane N, Stéphane F, Alexis B, Jonathan D, Marian C, Julian C, Bruno C, Alain R (2018) Improved water electrolysis using magnetic heating of FeC–Ni core–shell nanoparticles. *Nat Energy* 3:476–483
- Chun-Ren K, Jun-Sheng G, Yen-Hsun S, Jyh-Ming T (2016) The effect of silver nanoparticles/graphene-coupled  $\text{TiO}_2$  beads photocatalyst on the photoconversion efficiency of photoelectrochemical hydrogen production. *Nanotechnology* 27(43)
- Ciesla P, Kocot P, Mytych P, Stasicka Z (2004) Homogeneous photocatalysis by transition metal complexes in the environment. *J Mol Catal A Chem* 224:17–33
- Cox PA (1996) The surface science of metal oxides, chap. 5. Cambridge University Press, Cambridge, pp 158–246
- Dhanalakshmi KB, Latha S, Anandan S, Maruthamuthu P (2001) Dye sensitized hydrogen evolution from water. *Int J Hydrogen Energy* 26:669–674
- Dou Y, Egdell RG, Walker T, Law DSL, Beamson G (1998) N-type doping in CdO ceramics: a study by EELS and photoemission spectroscopy. *Surf Sci* 398:241–258
- El Nagggar AMA, Nassar IM, Gobara HM (2013) Enhanced hydrogen production from water via a photo-catalyzed reaction using chalcogenide d-element nanoparticles induced by UV light. *Nanoscale* 5:9994–9999
- Erdölyi A, Raskó J, Kecskés T, Tóth M, Dömök M, Baán K (2006) Hydrogen formation in ethanol reforming on supported noble metal catalysts. *Catal Today* 116:367–376
- Fan Z, Lu JG (2005) Zinc oxide nanostructures: synthesis and properties. *J Nanosci Nanotechnol* 5:1561–1573
- Fen Q, Zhiji H, Jeffrey JP, Michael YO, Kelly LS, Todd DK (2016) Photocatalytic hydrogen generation by CdSe/CdS nanoparticles. *Nano Lett* 16(9):5347–5352
- Fu N, Wu Y, Jin Z, Lu G (2009) Structural-dependent photoactivities of  $\text{TiO}_2$  nanoribbon for visible-light-induced  $\text{H}_2$  evolution: the roles of nanocavities and alternate structures. *Langmuir* 26:447–455
- Fujishima A, Honda K (1972) Electrochemical photolysis of water at a semiconductor electrode. *Nature* 238:37
- Fujishima A, Zhang X, Tryk DA (2008)  $\text{TiO}_2$  photocatalysis and related surface phenomena. *Surf Sci Rep* 63:515–582
- Furube A, Shiozawa T, Ishikawa A, Wada A, Domen K, Hirose C (2002) Femtosecond transient absorption spectroscopy on photocatalysts:  $\text{K}_4\text{Nb}_6\text{O}_{17}$  and  $\text{Ru}(\text{bpy})_3^{2+}$  intercalated  $\text{K}_4\text{Nb}_6\text{O}_{17}$  thin films. *J Phys Chem B* 106:3065–3072

- Galindo-Hernández F, Gómez R (2011) Degradation of the herbicide 2, 4-dichlorophenoxyacetic acid over  $\text{TiO}_2\text{-CeO}_2$  sol-gel photocatalysts: effect of the annealing temperature on the photoactivity. *J Photochem Photobiol A Chem* 217:383–388
- Ghosh M, Rao CNR (2004) Solvothermal synthesis of CdO and CuO nanocrystals. *Chem Phys Lett* 393:493–497
- Glasscock JA, Barnes PRF, Plumb IC, Savvides N (2007) Enhancement of photoelectrochemical hydrogen production from hematite thin films by the introduction of Ti and Si. *J Phys Chem C* 111(44):16477–16488
- Gu DE, Yang BC, Hu YD (2007) A novel method for preparing V-doped titanium dioxide thin film photocatalysts with high photocatalytic activity under visible light irradiation. *Catal Lett* 118:254–259
- Guan GQ, Kida T, Kusakabe K, Kimura K, Fang XM, Ma TL et al (2004) Photocatalytic  $\text{H}_2$  evolution under visible light irradiation on CdS/ETS-4 composite. *Chem Phys Lett* 385: 319–322
- Hashimoto K, Irie H, Fujishima A (2005)  $\text{TiO}_2$  photocatalysis: a historical overview and future prospects. *Jpn J Appl Phys* 44:8269–8285
- Hewitt CN, Jackson AV (2008) Handbook of atmospheric science: principles and applications, chap. 13. Wiley, pp 339–371
- Hoffman AJ, Yee H, Mills G (1992) Photoinitiated polymerization of methyl methacrylate using Q-sized zinc oxide colloids. *J Phys Chem* 96:5540–5546
- Hoffman AJ, Carraway ER, Hoffman MR (1994) Photocatalytic production of  $\text{H}_2\text{O}_2$  and organic peroxides on quantum-sized semiconductor colloids. *Environ Sci Technol* 28(5):776–785
- Hongjin L, Congcong W, Guocan L, Rebeckah B, Todd DK, Yongli G, Richard E (2017) Semiconductor quantum dot-sensitized rainbow photocathode for effective photoelectrochemical hydrogen generation. *PNAS* 114(43):11297–11302
- Hoshino K, Hirasawa Y, Kim S-K, Saji T, Katano J-I (2006) Bulk heterojunction photoelectrochemical cells consisting of oxotitanyl phthalocyanine nanoporous films and  $\text{I}_3^-/\text{I}^-$  redox couple. *J Phys Chem B* 110:23321–23328
- Ihara T, Miyoshi M, Iriyama Y, Matsumoto O, Sugihara S (2003) Visible-light-active titanium oxide photocatalyst realized by an oxygen-deficient structure and by nitrogen doping. *Appl Catal B Environ* 42:403–409
- Ikeda S, Fubuki M, Takahara YK, Matsumura M (2006) Photocatalytic activity of hydrothermally synthesized tantalite pyrochlores for overall water splitting. *Appl Catal A* 300:186–190
- Isaias J-R, Leticia MT-M, Christian G-S, Juan CB (2015) Photoelectrochemical hydrogen production using  $\text{SiC-TiO}_2\text{-Sm}_2\text{O}_3$  as electrode. *J Electrochem Soc* 162(4):H287–H293
- Izumi N, Junji A, Masayuki I, Ritsuro M, Yoshinori S, Kichiro K (1987) Characterization of the amorphous state in metamict silicates and niobates by EXAFS and XANES analyses. *Phys Chem Miner* 15:113–124
- Jacobson MZ (2005) Fundamentals of atmospheric modeling, chap. 21. Cambridge University Press, Cambridge, pp 681–708
- Jing D, Guo L (2006) A novel method for the preparation of a highly stable and active CdS photocatalyst with a special surface nanostructure. *J Phys Chem B* 110:11139–11145
- Jingyi X (2017) Preparation of ZnS-CdS nanocomposite for photoelectrochemical hydrogen production. *Int J Electrochem Sci* 12:2253–2261
- Karakitsou KE, Verykios XE (1995) Definition of the intrinsic rate of photocatalytic cleavage of water over Pt-RuO<sub>2</sub>/TiO<sub>2</sub> Catalysts. *J Catal* 152:360–367
- Karunakaran C, Dhanalakshmi R (2009) Selectivity in photocatalysis by particulate semiconductors. *Open Chem* 7:134–137
- Karunakaran C, Dhanalakshmi R, Gomathisankar P, Manikandan G (2010) Enhanced phenol-photodegradation by particulate semiconductor mixtures: interparticle electron-jump. *J Hazard Mater* 176:799–806
- Kawai T, Sakata T (1980) Photocatalytic hydrogen production from liquid methanol and water. *J Chem Soc Chem Commun* 15:694

- Ki HC, Yun MS (2017) Photoelectrochemical performance of CdS/ZnSe core/shell nanorods grown on FTO substrates for hydrogen generation. *J Electrochem Soc* 164:H382–H388
- Kim S, Hwang SJ, Choi WY (2005) Visible light active platinum-ion-doped TiO<sub>2</sub> photocatalyst. *J Phys Chem B* 109:24260–24267
- Kim SJ, Kim HH, Kwon JB, Lee JG, Beom-Hoan O, Lee SG, Lee EH, Park SG (2010) Novel fabrication of various size ZnO nanorods using hydrothermal method. *Microelectron Eng* 87:1534–1536
- Kim JK, Moon JH, Lee T-W, Park JH (2012) Inverse opal tungsten trioxide films with mesoporous skeletons: synthesis and photoelectrochemical responses. *Chem Commun* 48:11939–11941
- Kondo R, Okimura H, Sakai Y (1971) Electrical properties of semiconductor photodiodes with semitransparent films. *Jpn J Appl Phys* 10:1493–1659
- Langot P, Tommasi R, Vallae F (1996) Non-equilibrium hole relaxation dynamics in an intrinsic semiconductor. *Phys Rev B* 54:1775
- Li SX, Yu KM, Wu J, Jones RE, Walukiewicz W, Ager JW, Shan W, Haller EE, Lu H, Schaff WJ (2005) Fermi-level stabilization energy in group III nitrides. *Phys Rev B* 71:161201–161225
- Li HX, Xia RH, Jiang ZW, Chen SS, Chen DZ (2008) Optical absorption property and photo-catalytic activity of tin dioxide-doped titanium dioxides. *Chin J Chem* 26:1787–1792
- Liu H, Imanishi A, Nakato Y (2007) Mechanisms for photooxidation reactions of water and organic compounds on carbon-doped titanium dioxide, as studied by photocurrent measurements. *J Phys Chem C* 111:8603–8610
- Maeda K, Takata T, Hara M, Saito N, Inoue Y, Kobayashi H, Domen K (2005) ZnO solid solution as a photocatalyst for visible-light-driven overall water splitting. *J Am Chem Soc* 127:8286–8287
- Miyauchi M, Nakajima A, Watanabe T, Hashimoto K (2002) Photocatalysis and photoinduced hydrophilicity of various metal oxide thin films. *Chem Mater* 14:2812–2816
- Moliton A, Hiorns RC (2004) Review of electronic and optical properties of semiconducting of conjugated polymers: applications in optoelectronics. *Polym Int* 53:1397–1412
- Moradi S, Vossoughi M, Feilizadeh M, Zakeri SME, Mohammadi MM, Rashtchian D, Booshehri AY (2015) Photocatalytic degradation of dibenzothiophene using La/PEG-modified TiO<sub>2</sub> under visible light irradiation. *Res Chem Intermed* 41:4151–4167
- Morales-Torres S, Pastrana-Martinez LM, Figueiredo JL, Faria JL, Silva AMT (2012) Desing of grapheme-based TiO<sub>2</sub> photocatalysts—a review. *Environ Sci Pollut Res* 19:3676–3687
- Morales-Torres S, Pastrana-Martinez LM, Figueiredo JL, Faria JL, Silva AMT (2013) Graphene oxide-P25 photocatalysts for degradation of diphenhy-dramine pharmaceutical and methyl orange dye. *Appl Surf Sci*. <https://doi.org/10.1016/j.apsusc.2012.11.157>
- Murakami Y, Kasahara B, Nosaka Y (2007) Photoelectrochemical properties of the sulfur-doped TiO<sub>2</sub> film electrodes: characterization of the doped states by means of the photocurrent measurements. *Chem Lett* 36:330
- Naik B, Martha S, Parida KM (2011) Facile fabrication of Bi<sub>2</sub>O<sub>3</sub>/TiO<sub>2</sub>-xNx nanocomposites for excellent visible light driven photocatalytic hydrogen evolution. *Int J Hydrogen Energy* 36:2794–2802
- Nakamura I, Negishi N, Kutsuna S, Ihara T, Sugihara S, Takeuch K (2000) Role of oxygen vacancy in the plasma-treated TiO<sub>2</sub> photocatalyst with visible light activity for NO removal. *J Mol Catal A Chem* 161:205–212
- Nezamzadeh-Ejhih A, Banan Z (2011) A comparison between the efficiency of CdS nanoparticles/zeolite A and CdO/zeolite A as catalysts in photodecolorization of crystal violet. *Desalination* 279:146–151
- Nguyen N-T, Zheng D-D, Chen S-S, Chang C-T (2018) Preparation and photocatalytic hydrogen production of Pt-graphene/TiO<sub>2</sub> composites from water splitting. *J Nanosci Nanotechnol* 18 (1):48–55
- Ni M, Leung MK, Leung DY, Sumathy K (2007) A review and recent developments in photocatalytic water-splitting using TiO<sub>2</sub> for hydrogen production. *Renew Sustain Energy Rev* 11:401–425

- Ottone C, Laurenti M, Motto P, Stassi S, Demarchi D, Cauda VA (2014) ZnO nanowires: synthesis approaches and electrical properties, nanowires, synthesis, electrical properties and uses in biological systems, chap. 1. Nova Publisher, New York, NY, USA, pp 1–57
- Park JH, Domenico T, Dragel G, Clark R (1995) Development of electrical insulator coatings for fusion power applications. *Fusion Eng Des* 27:682–695
- Perera AGU, Sherriff RE, Francombe MH, Devaty RP (1992) Far infrared photoelectric thresholds of extrinsic semiconductor photocathodes. *Appl Phys Lett* 60:3168–3170
- Pérez-Larios A, Gómez R (2013) Hydrogen production using mixed oxides: TiO<sub>2</sub>-M (CoO and WO<sub>3</sub>). *Adv Invest Ing* 10:27–34
- Perliski LM, Solomon S (1993) On the evaluation of air mass factors for atmospheric near ultraviolet and visible absorption spectroscopy. *J Geophys Res Atmos* 98:10363–10374
- Pradhan AC, Martha S, Mahanta SK, Parida KM (2011) Mesoporous nanocomposite Fe/Al<sub>2</sub>O<sub>3</sub>-MCM-41: an efficient photocatalyst for hydrogen production under visible light. *Int J Hydrogen Energy* 36:12753–12760
- Salehi B, Mehrabian S, Ahmadi M (2014) Investigation of antibacterial effect of cadmium oxide nanoparticles on *Staphylococcus aureus* bacteria. *J NanoBioTechnol* 12:12–26
- Sathish M, Viswanathan B, Viswanath RP (2006) Alternate synthetic strategy for the preparation of CdS nanoparticles and its exploitation for water splitting. *Int J Hydrogen Energy* 31: 891–898
- Selvam NCS, Kumar RT, Yogeenth K, Kennedy LJ, Sekaran G, Vijaya JJ (2011) Simple and rapid synthesis of cadmium oxide (CdO) nanospheres by a microwave-assisted combustion method. *Powder Technol* 211:250–255
- Shim M, Guyot P (2000) N-type colloidal semiconductor nanocrystals. *Nature* 407:981–983
- Smith NA, Evans JE, Jones DR, Lord AM, Wilks SP (2015) Growth of ZnO nanowire arrays directly onto Si via substrate topographical adjustments using both wet chemical and dry etching methods. *Mater Sci Eng B* 193:41–48
- Sommerer TJ (1996) Model of a weakly ionized, low-pressure xenon dc positive column discharge plasma. *J Phys D Appl Phys* 29:769–780
- Song T, Zhang Z, Chen J, Ring Z, Yang H, Zheng Y (2006) Effect of aromatics on deep hydrodesulfurization of dibenzothiophene and 4, 6-dimethyldibenzothiophene over NiMo/Al<sub>2</sub>O<sub>3</sub> catalyst. *Energy Fuels* 20:2344–2349
- Soundarrajan C, Thomas N, Nicolas HV (2016) Silicon nanowire photocathodes for photoelectrochemical hydrogen production. *Nanomaterials* 6(8):144. <https://doi.org/10.3390/nano6080144>
- Sreethawong T, Yoshikawa S (2012) Impact of Pt loading methods over mesoporous-assembled TiO<sub>2</sub>-ZrO<sub>2</sub> mixed oxide nanocrystal on photocatalytic dye-sensitized H<sub>2</sub> production activity. *Mater Res Bull* 47:1385–1395
- Sreethawong S, Suzuki Y, Yoshikawa S (2005) Photocatalytic evolution of hydrogen over mesoporous TiO<sub>2</sub> supported NiO photocatalyst prepared by single step sol-gel process with surfactant template. *Int J Hydrogen Energy* 30:1053–1062
- Tak Y, Hong SJ, Lee JS, Yong K (2009) Solution-based synthesis of a CdS nanoparticle/ZnO nanowire heterostructure array. *Cryst Growth Des* 9:2627–2632
- Taylor SR (1964) Abundance of chemical elements in the continental crust: a new table. *Geochim Cosmochim Acta* 28:1273–1285
- Tong Y, Liu Y, Dong L, Zhao D, Zhang J, Lu Y, Shen D, Fan X (2006) Growth of ZnO nanostructures with different morphologies by using hydrothermal technique. *J Phys Chem B* 110:20263–20267
- Toru K, Morio N (2017) Cu-doped ZnS/zeolite composite photocatalysts for hydrogen production from aqueous S<sup>2-</sup>/SO<sub>3</sub><sup>2-</sup> solutions. *Chem Lett* 46(12):1797–1799
- Tseng IH, Jeffrey CSW (2004) Chemical states of metal-loaded titania in the photoreduction of CO<sub>2</sub>. *Catal Today* 97:113–119
- Walukiewicz W (1988) Fermi level dependent native defect formation: consequences for metals of semiconductor and semiconductor of semiconductor interfaces. *J Vac Sci Technol B* 6: 1257–1262

- Wang DF, Ye JH, Kako T, Kimura T (2006) Photophysical and photocatalytic properties of SrTiO<sub>3</sub> doped with Cr cations on different sites. *J Phys Chem B* 110:15824–15830
- Waymouth JF (1971) Electrical discharge lamps, chap. 14. Cambridge University Press, Cambridge, pp 331–347
- Wong MS, Fierro JG (2006) Metal oxides, chemistry and applications, chap. 17. Taylor & Francis, pp 543–568
- Wu CH, Chang CL (2006) Decolorization of reactive red 2 by advanced oxidation processes: comparative studies of homogeneous and heterogeneous systems. *J Hazard Mater* 128:265–272
- Xinjian S, Yong C, Kan Z, Jeong K, Dong YK, Ja KL, Sang HO, Jong KK, Jong HP (2014) Efficient photoelectrochemical hydrogen production from bismuth vanadate-decorated tungsten trioxide helix nanostructures. *Nat Commun* 5. Article number: 4775
- Yanping S, Carl JM, Karla RR, Enrique AR, Justin PL, Daniel R (2008) Carbon-doped In<sub>2</sub>O<sub>3</sub> films for photoelectrochemical hydrogen production. *Int J Hydrogen Energy* 33:5967–5974
- Yin S, Komatsu M, Zhang QW, Saito F, Sato T (2007) Synthesis of visible-light responsive nitrogen/carbon doped titania photocatalyst by mechanochemical doping. *J Mater Sci* 42: 2399–2404
- Yoong LS, Chong FK, Dutt BK (2009) Development of copper-doped TiO<sub>2</sub> photo-catalyst for hydrogen production under visible light. *Energy* 34:1652–1661
- Yu JC, Ho WK, Yu JG, Yip H, Wong PK, Zhao JC (2005) Efficient visible-light-induced photocatalytic disinfection on sulfur-doped nanocrystalline titania. *Environ Sci Technol* 39:1175–1179
- Zhang M, An T, Hu X, Wang C, Sheng G, Fu J (2004) Preparation and photocatalytic properties of a nanometer ZnO-SnO<sub>2</sub> coupled oxide. *Appl Catal A* 260:215–222
- Zheng XJ, Wei LF, Zhang ZH, Jiang QJ, Wei YJ, Xie B et al (2009) Research on photocatalytic H<sub>2</sub> production from acetic acid solution by Pt/TiO<sub>2</sub> nanoparticles under UV irradiation. *Int J Hydrogen Energy* 34:9033–9041
- Zou JJ, Liu C (2006) Preparation of NiO/SrTiO<sub>3</sub> with cold plasma treatment for photocatalytic water splitting. *Acta Phys Chim Sin* 22:926–931